Geometrical Thickness, Liquid Water Content, and Radiative Properties of Stratocumulus Clouds over the Western North Pacific

TADAHIRO HAYASAKA

Center for Atmospheric and Oceanic Studies, Faculty of Science, Tohoku University, Sendai, Japan

TERUYUKI NAKAJIMA

Center for Climate System Research, University of Tokyo, Tokyo, Japan

YASUSHI FUJIYOSHI, YUTAKA ISHIZAKA, AND TAKAO TAKEDA

Institute for Hydrospheric-Atmospheric Sciences, Nagoya University, Nagoya, Japan

MASAYUKI TANAKA

Center for Atmospheric and Oceanic Studies, Faculty of Science, Tohoku University, Sendai, Japan

(Manuscript received 18 March 1993, in final form 10 April 1994)

ABSTRACT

An algorithm was developed for retrieving cloud geometrical thickness from a measured liquid water path and equivalent width of 0.94-μm water vapor absorption band. The algorithm was applied to aircraft observations obtained by a microwave radiometer and a spectrometer in the winter of 1991 over the western North Pacific Ocean. Retrieved values of the cloud geometrical thickness are apt to be smaller than those observed by eye, especially for horizontally inhomogeneous clouds. Measured cloud albedos in the visible and near-infrared spectral region were also compared with calculated values. For homogeneous clouds there exists a single droplet size distribution that satisfies both spectral regions. However, for inhomogeneous clouds no single size distribution exists that satisfies the albedo observed in both spectral regions.

1. Introduction

Clouds in the earth's atmosphere are inhomogeneous and variable in space and time with various orders of scale and have significant influences on the earth's climate. In addition to horizontal variability in parameters such as cloud cover, vertical characteristics such as cloud top and base height, and therefore cloud thickness, are highly variable. Cloud geometrical thicknesses, as well as liquid water contents and other microphysical properties, are strongly coupled with the physical processes of cloud formation and dissipation (Brost et al. 1982a,b; Slingo et al. 1982; Hanson and Derr 1987; Albrecht et al. 1990; Blaskovic et al. 1991). Remote sensing techniques for retrieving cloud geometrical thicknesses and liquid water paths, or optical thicknesses, are quite effective in obtaining distributions of liquid water contents and extinction coefficients per unit volume over a wide area.

Corresponding author address: Dr. Tadahiro Hayasaka, Center for Atmospheric and Oceanic Studies, Faculty of Science, Tohoku University, Sendai 980, Japan.

Among the parameters describing physical properties of clouds, optical thicknesses have been successfully retrieved from measurements of solar radiation reflected by clouds in spectral regions without absorption (King 1987; Rossow 1989). Recently, an effective radius of cloud droplets and liquid water path have also been obtained by measuring the reflected radiation in near-infrared spectral regions that have significant absorption by cloud droplets (Rawlins and Foot 1990; Nakajima and King 1990; Nakajima et al. 1991). Liquid water paths have also been determined from measurements of microwave radiation (Wilheit and Chang 1980; Prabhakara et al. 1983; Takeda and Liu 1987; Jones and Vonder Haar 1990).

Cloud geometrical thicknesses, on the other hand, have been evaluated in situ for most cases after passing through clouds by aircraft or balloon (Stephens et al. 1978; Slingo et al. 1982; Herman and Curry 1984; Duda et al. 1991). Remote sensing techniques of the cloud geometrical thicknesses have not been fully discussed until recently. For optically thin clouds airborne lidars are useful, and successful results have been obtained (Spinhirne et al. 1989). The simultaneous usage of microwave and infrared radiation has also resulted

in estimates of ice water contents and geometrical thicknesses of thick clouds including large ice particles (Wu 1987). Moreover, reflected radiation in a nonabsorbing spectral region and that in the oxygen A band has been used to retrieve geometrical thickness of low-level stratus cloud (Asano and Shiobara 1992).

In the present study, a new algorithm is described to estimate the geometrical thickness and liquid water content of stratocumulus clouds by coupling microwave radiation at a frequency of 37 GHz with shortwave radiation in the spectral region of the 0.94-μm water vapor absorption band. This algorithm is based on a principle that the photon pathlength contained in the reflected radiation increases with an increase in cloud geometrical thickness for a fixed value of liquid water path. This algorithm is applied to the data obtained by airborne measurements during the Western North Pacific Cloud–Radiation Experiment in January 1991 conducted as part of the Japanese World Climate Research Programme. The accuracy and validity of the retrieval algorithm will be discussed in terms of averages and horizontal variations through a comparison with another measurement of microphysical, radiative, and thermodynamical properties of clouds.

2. Summary of aircraft observations

Two Cessna 404 aircraft were used for the observations. One aircraft was equipped with a spectrometer for measuring the spectrum of the water vapor absorption band in upward and downward radiance, a microwave radiometer for the liquid water path measurements, and pyranometers for the upward and downward radiative fluxes. The other aircraft was equipped with the Particle Measuring Systems (PMS) forward-scattering spectrometer probe (FSSP) for measuring cloud droplet size distributions for radii from 1 to 22.5 μm.

The spectrometer consists of a concave grating to disperse the solar spectrum and a plasma-coupled device array of 1024 elements as a detector. Spectrum data from 0.4 to 1.1 μm are obtained at a wavelength with an interval of 0.0007 μm and with the slit function specified by the widths of both slit and detector. The plasma-coupled device is an optical detector similar to a photodiode, based on the photoelectric effect. Incident light from nadir and zenith, and that through a quartz diffuser in the aircraft roof, are directed to the spectrometer by rotating a mirror. The angular field of view for the radiance measurements at nadir and zenith is 0.7° in the direction along the flight leg and less than 0.01° in the direction across the flight leg. The data were sampled at a maximum rate of 3 Hz, converted into 12-bit digital value, and recorded by a magnetic cassette tape. Data averaged over 1 s were used for the analysis in this study. The 37-GHz microwave radiometer was mounted on the same aircraft. It has a downward-looking parabola antenna with a full view angle of 4°. Data of brightness temperature at a sampling rate of 20 Hz were averaged for 1 s and recorded on a floppy disk.

Aircraft observations of stratocumulus clouds in the winter season were carried out over the western North Pacific Ocean to the southwest of Japan for the period from 10 to 28 January 1991. The winter stratocumulus is a typical cloud system frequently observed in this area where cold air masses from the Asian continent drive convection and form fairly uniform cloud systems at the top of the planetary boundary layer that lies over the warmer ocean. According to a map of 10-day-averaged sea surface temperature prepared by the Japan Meteorological Agency, the sea surface temperature in this area in January 1991 was 22°C. The average surface air temperature was 12.4°C at 0900 LST. The area was under the influence of a large stable anticyclone in a synoptic-scale condition.

Over this area of the Pacific Ocean in January, the cloud system observed is typically broken to overcast stratocumulus with layers at heights of 1–2 km. The cloud amount is usually large for low-level clouds but is less for higher-level clouds, particularly in January and February. When the clouds are formed by convection at the top of the planetary boundary layer under anticyclonic conditions, their tops are fairly flat under the strong inversion layer, whereas their bases are frequently complicated as though many broken clouds lay under the stratus. Figure 1 shows a typical example of atmospheric conditions observed on 18 January 1991. Air temperature and dewpoint temperature were measured by radiosonde. Cloud liquid water content and effective droplet radius were obtained by aircraft measurements. The difference between the height of the temperature inversion and the observed cloud-top height may result since these are based on measurements separated in time and space.

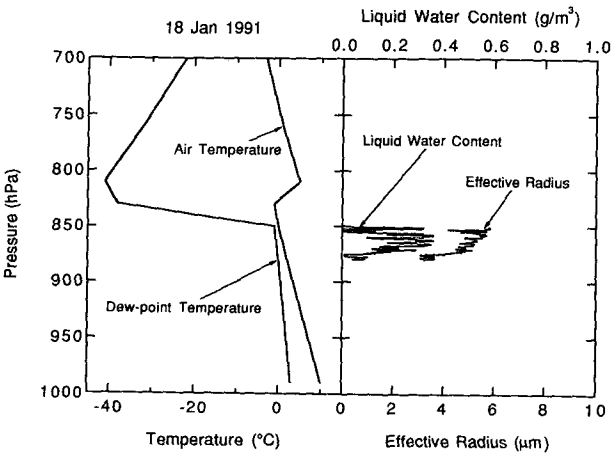

FIG. 1. Air temperature and dewpoint temperature measured by radiosonde, and cloud liquid water content and droplet effective radius obtained by aircraft measurement.

Almost all of the observed clouds consisted of liquid water droplets. In a few cases, frost was seen on the window of the aircraft near the top of the cloud during the penetration, suggesting the presence of ice particles. Ice particles are usually nonspherical and have a phase function, single scattering albedo, and asymmetry factor different from those of spherical particles. King (1987) has shown that the reflected radiance is sensitive to phase function, particularly for optically thin clouds. However, calculations of radiation in this study were performed based on the Mie theory for spherical particles because the scattering properties of ice particles are poorly understood and the concentration of ice particles in the observed clouds were small.

3. Retrieval of cloud geometrical thickness

This section presents a theoretical basis for the algorithm for retrieving cloud geometrical thickness from measurements of reflected solar radiation in a water vapor absorption band. This near-infrared spectral region includes gaseous absorption but no cloud particle absorption. The monochromatic gaseous absorption, A_ν at a wavenumber ν normalized by the solar constant, is described with the mass concentration ρ of absorbing gas per unit volume and the photon path distribution $f(l_\nu)$ for the reflected radiation as follows:

$$A_\nu = 1 - \int_0^\infty f(l_\nu) \exp(-k_\nu \rho l_\nu) dl_\nu, \qquad (1)$$

where k_ν is the mass absorption coefficient, and l_ν is the photon pathlength from the top of the atmosphere to the detector after multiple-scattering processes through the underlying cloud and subcloud layers. The photon path distribution is determined by the scattering extinction coefficient, the scattering phase function of cloud droplets, and the geometrical thickness of the cloud layer. In other words, the photon path distribution is determined by the liquid water content, droplet size distribution, and geometrical thickness. The liquid water content per unit volume is equivalent to the liquid water path in the column of cloud layer. This leads to the possibility of estimating the geometrical thickness of cloud layer by measuring the reflected solar radiation in the gaseous absorbing spectral region if parameters other than geometrical thickness are known.

In this study, total absorption of a radiance from nadir in the spectral region of the water vapor 0.94-μm absorption band and liquid water path obtained with a 37-GHz microwave radiometer are used. The total absorption by water vapor in the spectral interval between wavenumbers ν_1 and ν_2 is evaluated with an equivalent width defined as

$$W = \int_{\nu_1}^{\nu_2} A_\nu d\nu, \qquad (2)$$

which is the width of a rectangular band having the same absorption area whose center is completely absorbed. The equivalent width increases with increasing cloud geometrical thickness through an increase in photon pathlength, and vice versa. To obtain the liquid water path from measured microwave radiances, the method by Takeda and Liu (1987) was used in this study. This method uses cloud emissivity dependence on the liquid water path. The emission from the cloud is obtained by taking a difference in the radiation measured over clouds and that over clear regions. A brief outline of the retrieval of liquid water path is described in the appendix.

Reflected radiance and equivalent width in the 0.94-μm water vapor absorption band were calculated with various cloud geometrical thicknesses. For the calculation, a six-layer atmosphere with four layers in the cloud and a single layer above and below the cloud, respectively, was used. The discrete ordinates method of Nakajima and Tanaka (1986, 1988) was used for radiative transfer calculations. Saturated relative humidity was assumed throughout the cloud layer and 80% relative humidity for the subcloud layer. Although the relative humidity of subcloud layer was not measured in situ by the aircraft, the average relative humidity of the surface, the 900- and 850-mb levels in January 1991, was calculated to be 78.7% from the radiosonde measurements at Naze Observatory of the Japan Meteorological Agency. Absorption by water vapor in the reflected radiance was calculated for the spectral region from 11 500 (0.8696) to 10 100 cm^{-1} (0.9901 μm) with the exponential-sum-fitting coefficients provided by Asano and Uchiyama (1987). The influences of temperature and pressure on the absorption were taken into account by using the layer average of the respective quantities. The amount of water vapor above the cloud was adjusted to fit the calculated total absorption of solar radiation in the 0.94-μm water vapor band to the observed. Considering that liquid water content generally increases with increasing height, 40%, 30%, 20%, and 10% of the total liquid water content were distributed in the four layers from cloud top to base. The droplet size distribution was fixed for all cloud layers with a lognormal size distribution:

$$n(r) = \frac{C}{(2\pi)^{1/2} r \ln\sigma} \exp\left[\frac{-(\ln r - \ln r_0)^2}{2(\ln\sigma)^2}\right]. \qquad (3)$$

The dispersion parameter σ was assumed to be 1.40, and the mode radius r_0 was assumed to be 5.4 μm since almost all of the mode radii observed by PMS FSSP in the upper layer of clouds exist in a range between 3.6 and 7.2 μm. With these parameters, the effective radius

$$r_e = \frac{\int_0^\infty r^3 n(r) dr}{\int_0^\infty r^2 n(r) dr} \qquad (4)$$

was calculated as 7.1 μm, while the observed values were 4.7–9.4 μm. The complex refractive index of liquid water in the 0.94-μm spectral region was assumed to be $1.33 - 1.0 \times 10^{-6}\, i$, from the compilation of Hale and Querry (1973). Changing the cloud geometrical thickness with other parameters fixed, the equivalent width in the radiance reflected from clouds was calculated. In this procedure, the thickness of the planetary boundary layer was held constant as the cloud-top height is fixed at 800 mb. Therefore, changes in the ratio of cloud layer to subcloud layer were expressed as a function of cloud thickness.

The cloud geometrical thickness was estimated by comparing the calculated equivalent width to the observed. The equivalent width was calculated using temperature, water vapor, and liquid water path measured by radiosonde and aircraft on 16 January 1991. A strong inversion layer was observed at the top of the extended stratiform cloud layer (800 mb). The cloud formed at the top of the planetary boundary layer. Above this level, the air mass was fairly dry under an anticyclonic condition. Figure 2 shows calculated results of the equivalent width as a function of liquid water path and geometrical thickness. The equivalent width, due to absorption of the incident radiation by the water vapor above the cloud layer, was previously subtracted from the total equivalent width so that an increment of equivalent width by the cloud layer and subcloud layer is shown. Figure 2 indicates that the equivalent width is more sensitive to the cloud geometrical thickness than to the liquid water path. The results suggest that the photon pathlength in the reflected radiance varies little with liquid water path for the same geometrical thickness of the cloud layer.

Instead of liquid water path, the optical thickness of cloud is useful if it is available. The cloud optical thickness τ is related to liquid water path w with a relationship $\tau = 3w/2\rho r_e$ (Stephens 1978). According to a simple Monte Carlo simulation, an average photon pathlength is determined from cloud geometrical thickness and optical thickness, independent of the droplet size distribution. In this study, liquid water path, not optical thickness, was used, leading to a dependency of the retrieval accuracy to cloud droplet size distribution. Since the change of droplet size almost corresponds to that of the liquid water path in Fig. 2, it is found that the droplet size does not affect the geometrical thickness retrieval of thin clouds so much but does affect the retrieval of thick clouds.

The sensitivity of the retrieved geometrical thickness to several parameters was examined. An error of about 100 m in 400-m geometrical thickness was found to be caused by 20% uncertainty in water vapor amount in the cloud and subcloud layers. Consequently, this parameter has a large influence on the retrieval of geometrical thickness. This uncertainty corresponds to about 100% error in liquid water path. The liquid water path was estimated within an accuracy of 30% from the microwave radiation measurements, so that the uncertainty in geometrical thickness due to liquid water path seems to be small. On the other hand, 50% uncertainty in water vapor amount above the cloud causes about 10% uncertainty in the equivalent width to be measured. This in turn causes 100-m uncertainty in geometrical thickness retrieval in this case. In this study, the absorption of solar radiation by the upper layer above the cloud was measured directly with the same spectrometer, and the measurement was obtained with

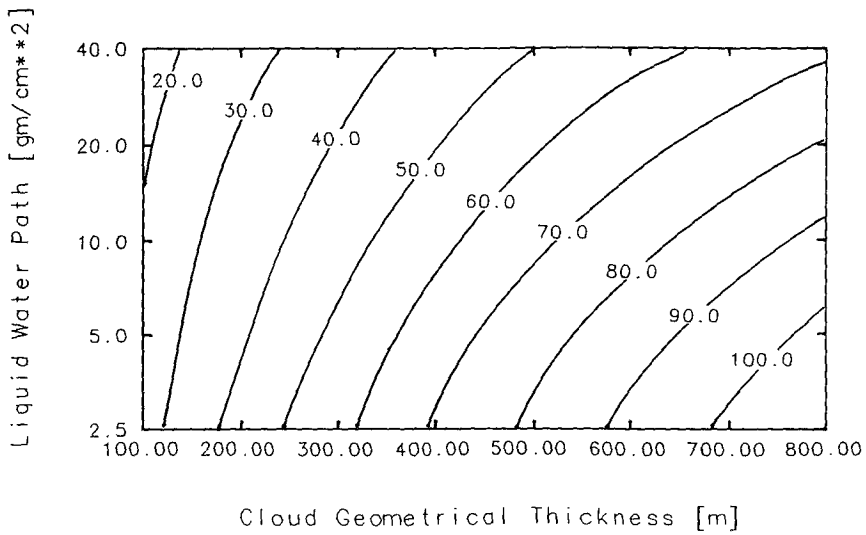

FIG. 2. Contours of equivalent width of the 0.94-μm water vapor absorption band in a radiance reflected by clouds. The equivalent width was calculated as a function of cloud liquid water path and cloud geometrical thickness with a water vapor profile and cloud-top altitude observed on 16 January 1991.

an accuracy of several percent. However, the effect of water vapor above the cloud should be carefully taken into account in the application of this method to satellite remote sensing. Because the analysis was performed on the assumption of plane-parallel atmospheric layer, horizontal inhomogeneities may cause errors in the retrieval of cloud geometrical thicknesses. This problem will be discussed later in section 4.

Figure 3 shows an example of time series of liquid water path, upward radiance at 0.87 μm with an arbitrary unit and equivalent width of the 0.94-μm water vapor absorption band, respectively, observed above the cloud on 16 January 1991. The abscissa indicates the elapsed time in seconds. The aircraft flew at a speed of 70 m s^{-1} so that the full scale of the abscissa corresponds to 21 km. Although the cloud appeared visually to be a homogeneous stratiform cloud, it was found that liquid water path had an increasing trend and was variable at small scales. The trend of liquid water path is consistent with the upward radiance at 0.87 μm as a whole. Since the imaginary index of refraction of liquid water at the wavelength 0.87 μm is quite small, that is, 3.9×10^{-7} (Hale and Querry 1973), cloud particle absorption of radiation is negligible. Accordingly, the radiance at this wavelength is strongly correlated with optical thickness, independent of droplet particle radius; it is also correlated with liquid water path if the particle radius does not change along the observed aircraft track. Some differences in detail between the liquid water path and radiance at 0.87 μm can be attributed to the difference in field of view of both instruments and to the effect of shadowing in the radiance at 0.87 μm rather than particle radius variation. The upward shortwave radiance reflected by the cloud layer is strongly affected by the cloud-top morphology, solar direction, and viewing direction, while the microwave radiance is hardly affected by these variations.

The radiance at 0.87 μm is inversely related to the equivalent width. It is apparent from the comparison of these two parameters that the photon pathlength distribution of radiance in a bright area is shorter than that in a dark area. The dark area at 0.87 μm corresponds to either low liquid water content or cloud shading. Upwelling photons from the shaded area seemed to be transported along a long path caused by multiple scattering after incidence on the inhomogeneous cloud in another area illuminated by direct solar radiation. As an extreme example, a large peak in equivalent width observed at 30 s of elapsed time in Fig. 3 can be ascribed to a cloud hole with small liquid water path where the upward radiance includes much more long photon paths passed through ambient clouds. Averages of the equivalent width of the first half and the second half in Fig. 3 are 48.0 and 39.8 cm^{-1}, respectively. Referring to the result of equivalent width calculated for this day as shown by Fig. 2, average cloud geometrical thicknesses were estimated as 273 and 231 m, respectively. These are slightly small compared to the cloud geometrical thickness of 240–400 m observed visually in crossing the cloud.

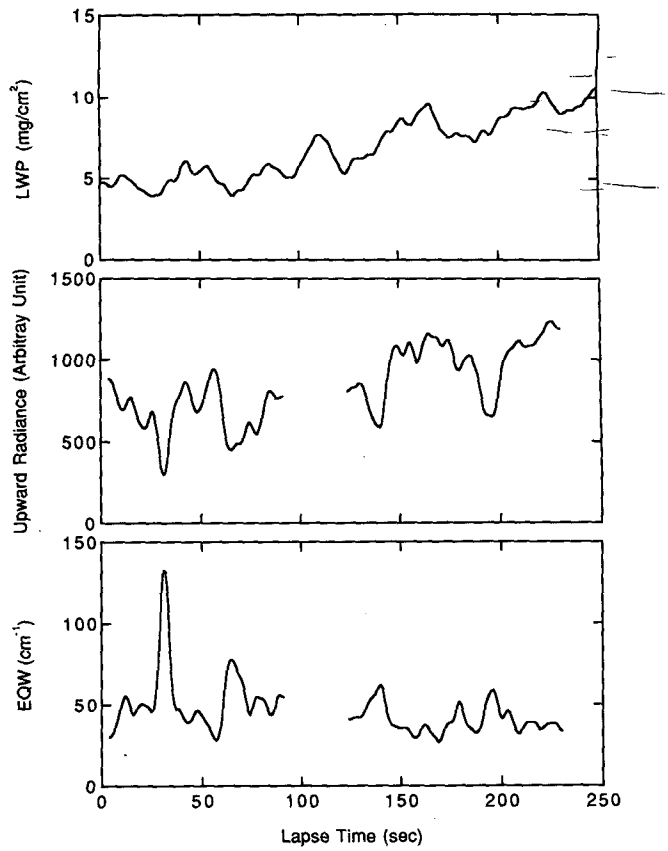

FIG. 3. Time series of cloud liquid water path, upward radiance reflected from clouds at a wavelength of 0.87 μm and equivalent width of the 0.94-μm water vapor absorption band in the radiance from clouds observed on 16 January 1991.

4. Geometrical thickness, liquid water content, and albedo of cloud

a. Case studies on the extended stratiform clouds

The remote sensing algorithm developed in this study was applied to six datasets of extended stratiform clouds. The cloud geometrical thickness was retrieved and liquid water content was estimated from liquid water path and geometrical thickness of the cloud. The liquid water path, equivalent width, and cloud geometrical thickness obtained are shown in Table 1. The ranges of geometrical thicknesses observed visually from the aircraft are also included in this table. These values were obtained when the aircraft for microphysical measurements passed through the cloud layer. The geometrical thicknesses retrieved with the algorithm in this study are slightly smaller than those observed visually on 16 and 18 January, and conspicuously smaller

TABLE 1. Observed cloud liquid water path (LWP), equivalent width of the water vapor 0.94-μm absorption band (EQW), and cloud geometrical thickness retrieved with the algorithm in this study and that observed by eye.

Date	Time	LWP (mg cm^{-2})	EQW (cm^{-1})	Thickness (m)	
				Retrieved	Observed
14 January 1991	1141:35–1143:05	13.7	51.1	471	600–1200
14 January 1991	1144:24–1145:54	12.2	49.4	443	600–1200
16 January 1991	1333:04–1334:30	6.6	48.0	273	240–400
16 January 1991	1334:59–1336:50	9.8	39.8	231	240–400
18 January 1991	1349:48–1351:00	24.2	31.8	234	210–430
27 January 1991	1315:14–1315:47	14.3	69.0	403	500–800

than those observed on 14 and 27 January. On the latter two days (14 and 27 January), the clouds were stratocumuli and the irregularity and inhomogeneity of the cloud tops and bases were much larger than on the other two days. In such conditions, the cloud-top height observed visually may be higher than the geometrically averaged height of the cloud top, and the base height observed visually may be lower than the geometrically averaged base height. Consequently, visual observations in these cases would tend to overestimate the geometrical thickness. However, the clouds on the former two days (16 and 18 January) were extended stratus, which makes it possible to use the plane-parallel assumption, and the underestimate of cloud geometrical thickness may be due to other reasons such as less than 100% relative humidity in the cloud layer.

Table 2 shows the liquid water content obtained from the liquid water path and geometrical thickness, and that from the PMS FSSP droplet spectrometer. The "RS" column indicates the liquid water content obtained by using the geometrical thickness retrieved from the remote sensing algorithm developed in this study, while the "eye (min)" and "eye (max)" columns give minimum and maximum values, respectively, of the geometrical thickness as obtained by visual observation. Clouds observed in this study varied systematically on different days. Stratus clouds with thinner geometrical thickness and large liquid water content were obtained on 18 January. Measurements on 14, 16, and 27 January indicate liquid water content in the range generally observed for stratocumulus or stratus clouds. The liquid water content obtained by remote sensing was evaluated as an average for the whole cloud layer without consideration of its vertical distribution. Since clouds generally have liquid water content increasing with increasing height, the liquid water content may locally become larger in the upper layer of cloud than that in the lower layer.

Cloud liquid water content was also measured by the PMS FSSP droplet spectrometer, except on 16 January. On that day the observations were performed by only one aircraft. The anomalously large liquid water content on 18 January was not consistent with the measurements by the PMS FSSP. Consistency between both methods was obtained on 14 and 27 January. The accuracy of liquid water content measured by the PMS FSSP depends on calibration of particle size and sampling volume. The particle size is reliable if the particle radius is not so large (Hovenac and Lock 1993). The sampling volume is determined from the effective sample area and airspeed in measurements. The accuracies of effective area and airspeed were estimated to be 10% in this study. A recent intercomparison of the cloud liquid water content between PMS FSSP and another instrument has shown agreement within 15% (Gerber 1991). Therefore, the large liquid water content on 18 January is not ascribed to uncertainty in the PMS FSSP measurement. A possible explanation is that the cloud volume observed for radiation measurements from one aircraft is not necessarily the same as that observed for microphysical measurements from the other aircraft.

TABLE 2. Cloud liquid water content estimated from the liquid water path and cloud geometrical thickness, measured in situ in the cloud, and estimated from adiabatic condensation.

Date	Liquid water content (g m^{-3})					
	RS	Eye (max)	Eye (min)	FSSP (avg)	FSSP (max)	Adiabatic
14 January 1991	0.291	0.228	0.114	0.28	0.61	1.2
14 January 1991	0.275	0.203	0.102	0.28	0.61	1.2
16 January 1991	0.242	0.275	0.165	—	—	0.7
16 January 1991	0.424	0.408	0.245	—	—	0.7
18 January 1991	1.034	1.152	0.563	0.20	0.48	0.7
27 January 1991	0.355	0.286	0.179	0.18	0.50	1.0

The maximum liquid water content can be calculated with the vertical profile of air temperature using the assumption that the saturated air parcel rises up adiabatically from cloud base to cloud top. The liquid water content estimated from adiabatic ascent was 0.7 g m^{-3} at the cloud top; this value is smaller than that estimated by the liquid water path and geometrical thickness retrieved in this study or observed visually. On days other than 18 January, cloud liquid water content retrieved was less than the adiabatic liquid water content. Consequently, the anomalously large value of the observed liquid water content on 18 January cannot be explained by adiabatic ascent.

Measurements of cloud albedo in the visible and near-infrared spectral regions were also obtained, and the consistency with liquid water path was examined. With the liquid water path obtained from microwave radiometry, the albedo was calculated for the visible region from 0.3 to 0.7 μm and for the near-infrared region from 0.7 to 3.0 μm. Scattering by molecules and cloud droplets, and gaseous absorption by ozone and water vapor were included. The same schemes as those used in section 2 were used for the radiative transfer (Nakajima and Tanaka 1986) and the exponential-sum coefficients of water vapor absorption (Asano and Uchiyama 1987).

Table 3 shows cloud albedo in the visible and near-infrared regions both calculated and measured. The small and large droplet size distribution corresponding to $r_0 = 3.6$ μm and $r_0 = 7.2$ μm in Eq. (3), which was used for the calculation, are denoted by "S" and "L", respectively. Pyranometer observations are indicated by "O." The observed albedo in the visible region is consistent with that in the near-infrared region on 16 and 18 January. If the liquid water path is correct, the optimal mode radius r_0 is estimated as 7.2 and 5.2 μm for describing albedos observed on 16 January and 3.6 μm on 18 January. These mode radii satisfy both visible and near-infrared albedos. These results appear to support the large liquid water path on 18 January observed with the microwave radiometer. On the other hand, the visible and near-infrared albedos on 14 and 27 January are not consistent with each other. The visible albedos on these days agree with the observed liquid water path if an appropriate size distribution is assumed. However, the near-infrared albedo and visible albedo do not agree if the same size distribution is used. The near-infrared albedo is lower than that expected from the visible albedo, and larger droplets and/or more abundant water vapor are necessary to give the lower values of near-infrared albedos. Since the total liquid water path is fixed by the measurement with the microwave radiometer, the observed visible albedo cannot be explained with such a larger droplet size distribution.

A characteristic difference between the radiatively consistent and inconsistent clouds is horizontal homogeneity. The clouds observed on 16 and 18 January were stratiform clouds close to plane-parallel condition, while those on 14 and 27 January were horizontally inhomogeneous stratocumulus clouds. With respect to the effect of cloud inhomogeneity, Coakley and Davies (1986) pointed out that the backward-reflected radiance in the near-infrared region increases with increasing cloud aspect ratio, defined as a ratio of the vertical size to the horizontal, while in the visible region this is reversed. Therefore, the spatial inhomogeneity effect is inadequate to explain the reason of discrepancy in the radiatively inconsistent clouds.

b. Horizontally inhomogeneous clouds

An advantage of the remote sensing algorithm used in this study is that it provides cloud geometrical thickness and liquid water content simultaneously from the measurements above clouds. The aircraft observation makes it possible to obtain spatial structures, particularly horizontal variations. Combining these characteristics for the analysis, two examples of the horizontal variation of cloud structure derived from the observations on 18 and 14 January will now be discussed.

An example of the horizontal variation of cloud is shown in Fig. 4 in terms of liquid water path and equivalent width. In this flight leg on 18 January, liquid water path gradually decreased from about 30 mg cm^{-2} to less than 10 mg cm^{-2} in a distance of 12–13 km. The equivalent width shows an almost constant value. This suggests that the cloud geometrical thickness does

TABLE 3. Calculated and observed cloud albedo in the visible (VIS) and near-infrared (NIR) spectral regions. The S and L in the parentheses indicate small ($r_0 = 3.6$ μm) and large ($r_0 = 7.2$ μm) mode radii in droplet volume spectrum. Equation (3) used in the calculation, while O indicates observed value.

Date	LWP (mg cm^{-2})	Albedo (%)					
		VIS(S)	VIS(L)	VIS(O)	NIR(S)	NIR(L)	NIR(O)
14 January 1991	13.7	80.0	65.7	79.5	70.1	55.6	61.5
14 January 1991	12.2	78.5	63.7	76.3	69.0	54.1	59.6
16 January 1991	6.6	70.5	54.7	54.3	64.6	48.2	48.2
16 January 1991	9.8	77.3	62.6	67.8	69.8	54.7	60.2
18 January 1991	24.2	87.8	77.1	87.7	78.0	66.7	76.8
27 January 1991	14.3	81.9	68.1	74.7	73.7	59.6	61.9

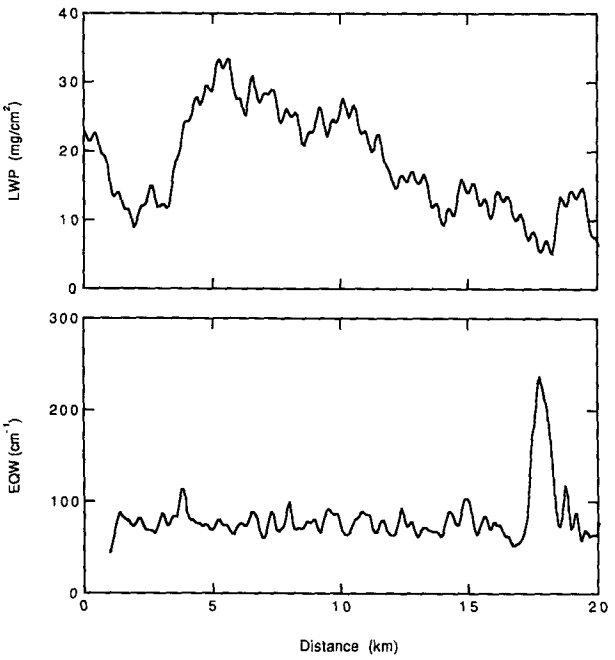

FIG. 4. Horizontal variation of cloud liquid water path and equivalent width of the 0.94-μm water vapor absorption band in the radiance from clouds observed on 18 January 1991.

not change as much along the flight leg as discussed for Fig. 3 in section 3. The retrieved geometrical thicknesses are 247 and 192 m corresponding to the liquid water paths 30 and 10 mg cm^{-2}, respectively. During a 67% decrease in liquid water path, the geometrical thickness decreased only 22% and, consequently, the vertically averaged liquid water content in a unit volume decreased from 1.21 to 0.52 g m^{-3} in the distance of about 10 km. The retrieved geometrical thickness and liquid water content of the cloud are schematically indicated by Fig. 5 corresponding to the distance from 5 to 10 km in Fig. 4.

A decrease in liquid water content with a decrease in cloud geometrical thickness was also observed by Blaskovic et al. (1991) from ground-based observations at San Nicolas Island that were carried out as a part of the First ISCCP (International Satellite Cloud Climatology Program) Regional Experiment. Such variations of clouds at San Nicolas Island are coupled with diurnal variations of various processes, especially of radiation. The horizontal scales of geometrical thickness and liquid water content variations obtained in this study were small and resulted from the convection formed in a large-scale atmospheric condition. Geometrical thicknesses and liquid water contents were found to be uncorrelated with radiation in this study. This result differs from that observed at San Nicolas Island.

Figure 6 also shows variations of liquid water path and the equivalent width of the 0.94-μm water vapor absorption band in a flight leg on 14 January. In the record of liquid water path the variation is roughly

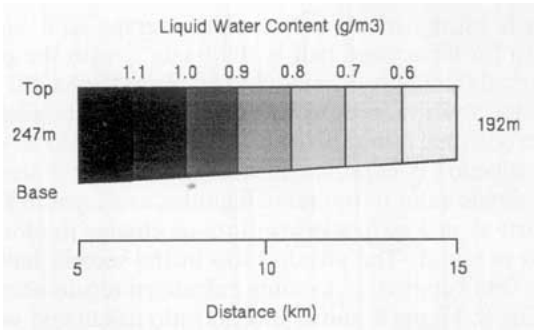

FIG. 5. Schematic of the retrieved cloud geometrical thickness and liquid water content where the distance corresponds to that in Fig. 4.

similar to that shown in Fig. 4 (18 January). In the equivalent width a large change is found at a distance of about 19 km. From the data of upward radiance at 0.87 μm measured by the spectrometer and video images, clouds in the first half are almost overcast and have rather small variation in equivalent width, and therefore in geometrical thickness. In the second half, clouds are horizontally inhomogeneous and partly broken. From results obtained by applying the algorithm in this study that assumes a plane-parallel cloud to these data, the geometrical thickness in the second half seems to be apparently much larger than that in the first half. It looks like a "jump" in cloud thickness without a corresponding change in the liquid water path. The averaged equivalent width for the first half is 50.3 cm^{-1} and the corresponding geometrical thick-

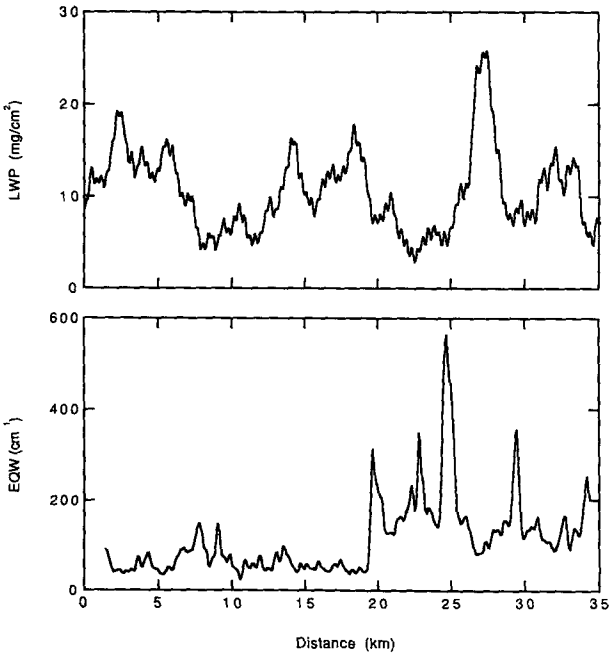

FIG. 6. Same as in Fig. 4 except for 14 January 1991.

ness is estimated as 463 m. The average equivalent width for the second half is 109.6 cm^{-1}, with the geometrical thickness estimated to be more than 1200 m.

If the absorption by water vapor increases, the albedo ratio (defined as a ratio of near-infrared albedo to visible albedo) is expected to decrease. Figure 7 shows the albedo ratio in the same flight leg as shown in Fig. 6. Just as in Fig. 6, a discontinuous change in albedo ratio is found. The albedo ratio in the second half is very small compared to some calculated results shown in Fig. 8. Figure 8 shows albedo ratio calculated with size distributions given by Eq. (3) assuming three values of mode radius (i.e., r_0 = 3.6, 7.2, and 10.8 μm). The observed albedo ratio even in the first half in Fig. 7 is small and the existence of large droplets is expected from Fig. 8. Moreover, an albedo ratio less than 0.75 in the second half is not acceptable using cloud droplet sizes from Fig. 8. Since the photon pathlength in the second half is supposed to increase from the equivalent width measurements, the albedo ratio with a large geometrical thickness of 2 km was calculated in order to increase absorption by water vapor. This result is indicated by dotted line in Fig. 8. However, the observed albedo ratio is still not consistent with the calculated value, which assumes a plane-parallel atmosphere and normal droplet sizes. The remaining possibilities are an additional increase of photon pathlength in broken clouds compared with plane-parallel clouds and/or the existence of giant droplet particles such as drizzle.

In any case, it is obvious that the cloud structure changed at a distance of 19 km, where the stratus cloud deck changed to a broken and complicated cloud system. As presented by Coakley and Davies (1986), the near-infrared reflectance, and thereby the near-infrared albedo, is apt to increase with an increase in aspect ratio. Their results were obtained with an assumed size distribution and water vapor amount. This study suggests that the changes in cloud microphysics can overcome the influence of cloud brokenness. The low albedo ratio observed in this study, as shown in Table 3 and Fig. 7, has the same properties as pointed out by Hignett (1987) and may provide a suggestion for solving the cloud absorption anomaly problem (Stephens and Tsay 1990).

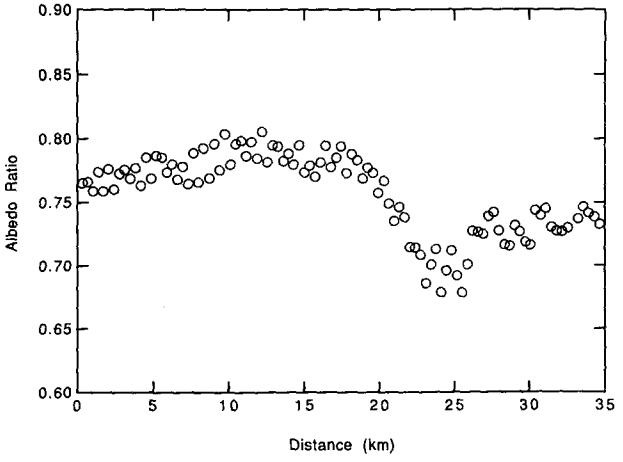

FIG. 7. Albedo ratio defined as a ratio of near-infrared albedo to visible albedo observed corresponding to the same flight leg as shown in Fig. 6.

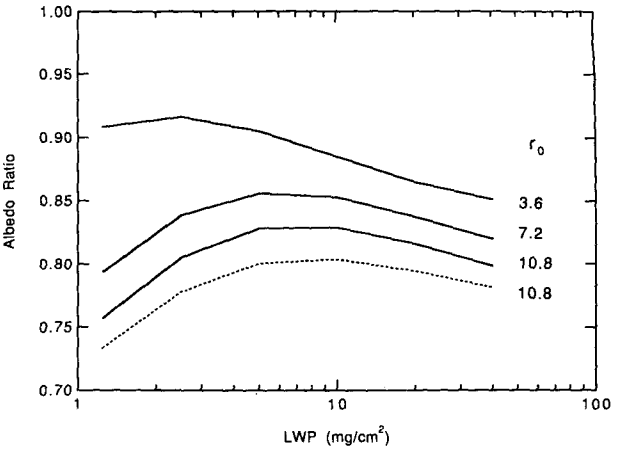

FIG. 8. Albedo ratio calculated with the atmospheric condition of 14 January for the comparison with the observation shown in Fig. 7. The mode radius of cloud droplet size distribution r_0 is given by Eq. (3). The dotted line shows the result with an assumption of twofold geometrical thickness of clouds.

5. Summary

Based on a relationship between the amount of absorption for water vapor in the 0.94-μm band and cloud geometrical thickness for a fixed liquid water path, an algorithm was developed to retrieve cloud geometrical thickness. The algorithm was applied to radiation data obtained over the western North Pacific Ocean from an aircraft equipped with a microwave radiometer and spectrometer. The retrieved cloud geometrical thickness was shown to be smaller than that observed by eye, especially for the horizontally inhomogeneous clouds. Uncertainties in the visual recognition of cloud base may contribute to this discrepancy.

The cloud liquid water content was estimated from the liquid water path and cloud geometrical thickness retrieved with the algorithm developed in this study as well as for visual cloud thickness. Values generally were reasonable except an anomalously large liquid water content found on 18 January. Compared with that measured by the PMS FSSP or even with that estimated as a maximum value using an assumption of adiabatic condensation for a rising parcel of saturated air at cloud base, the retrieved liquid water content was large.

Measurements of visible and near-infrared cloud albedo were also obtained. For the horizontally homogeneous clouds, both visible and near-infrared albedos were found to be consistent with each other for a single

liquid water path and a single cloud droplet size distribution. However, for the inhomogeneous clouds, these were not consistent (i.e., the near-infrared to visible albedo ratio observed was smaller than the calculated albedo ratio). This result may suggest that the spatial inhomogeneities or complicated structures of cloud result in the lower albedo ratio than that expected from the theoretical consideration with the plane-parallel cloud assumption.

Acknowledgments. We would like to thank Dr. G. Liu for his support in the analysis of microwave radiometer data to obtain cloud liquid water content. Mr. N. Kikuchi is acknowledged for his assistance in the analyses of radiation data. Dr. B. A. Wielicki is also acknowledged for valuable comments on this paper. We are grateful to Dr. K. Higuchi and anonymous reviewers for their critical readings of the manuscript. This research was supported by the Ministry of Education, Science and Culture of Japan.

APPENDIX

Retrieval of Liquid Water Path

In the 37-GHz spectral region, the scattering by cloud droplet can be neglected since the droplet radius is much smaller than the wavelength, and therefore, the mass absorption coefficient is important and given by

$$A = \frac{6\pi}{\lambda\rho} \operatorname{Im}\left(-\frac{m^2 - 1}{m^2 + 2}\right), \tag{A1}$$

where λ, ρ, and m are the wavelength of microwave, the density, and the complex refractive index of liquid water, respectively. Assuming that the temperature of cloud T_c is constant, the brightness temperature of cloud T_{bc} is expressed by

$$T_{bc} = T_c[1 - \exp(-\tau)], \tag{A2}$$

where

$$\tau = Aw. \tag{A3}$$

Tau (τ) is optical thickness for a liquid water path w and, therefore, an effective emissivity of the cloud is given by

$$\epsilon_c = \frac{T_{bc}}{T_c} = 1 - \exp(-\tau). \tag{A4}$$

From Eqs. (A1)–(A4), the liquid water path of the cloud is determined as

$$w = \frac{1}{A} \ln\left(\frac{1}{1 - \epsilon_c}\right). \tag{A5}$$

In the practical analysis, additional information such as the temperature of antenna is necessary to obtain the emissivity.

REFERENCES

Albrecht, B. A., C. W. Fairall, D. W. Thomson, A. B. White, J. B. Snider, and W. H. Schubert, 1990: Surface-based remote sensing of the observed and the adiabatic liquid water content of stratocumulus clouds. *Geophys. Res. Letters,* **17,** 89–92.

Asano, S., and A. Uchiyama, 1987: Application of an extended ESFT method to calculation of solar heating rates by water vapor absorption. *J. Quant. Spectrosc. Radiat. Transfer,* **38,** 147–158.

——, and M. Shiobara, 1992: Estimation of cloud parameters from spectral reflectances measured by airborne multi-channel cloud pyranometers. Tech. Rep. No. 29, Meteorological Research Institute, Japan Meteorological Agency, 152–167.

Blaskovic, M., R. Davies, and J. B. Snider, 1991: Diurnal variation of marine stratocumulus over San Nicolas Island during July 1987. *Mon. Wea. Rev.,* **119,** 1469–1478.

Brost, R. A., D. H. Lenschow, and J. C. Wyngaard, 1982a: Marine stratocumulus layers. Part I: Mean conditions. *J. Atmos. Sci.,* **39,** 800–817.

——, J. C. Wyngaard, and D. H. Lenschow, 1982b: Marine stratocumulus layers. Part II: Turbulence budgets. *J. Atmos. Sci.,* **39,** 818–836.

Coakley, J. A., Jr., and R. Davies, 1986: The effect of cloud sides on reflected solar radiation as deduced from satellite observations. *J. Atmos. Sci.,* **43,** 1025–1035.

Duda, D. P., G. L. Stephens, and S. K. Cox, 1991: Microphysical and radiative properties of marine stratocumulus from tethered balloon measurements. *J. Appl. Meteor.,* **30,** 170–186.

Gerber, H., 1991: Direct measurement of suspended particle volume concentration and far-infrared extinction coefficient with a laser-diffraction instrument. *Appl. Opt.,* **30,** 4824–4831.

Hale, G. M., and M. R. Querry, 1973: Optical constants of water in the 200-nm to 200-mm wavelength region. *Appl. Opt.,* **12,** 555–563.

Hanson, H. P., and V. E. Derr, 1987: Parameterization of radiative flux profiles within layer clouds. *J. Climate Appl. Meteor.,* **26,** 1511–1521.

Herman, G. F., and J. A. Curry, 1984: Observational and theoretical studies of solar radiation in Arctic stratus clouds. *J. Climate Appl. Meteor.,* **23,** 5–24.

Hignett, P., 1987: A study of the short-wave radiative properties of marine stratus: Aircraft measurements and model comparisons. *Quart. J. Roy. Meteor. Soc.,* **113,** 1011–1024.

Hovenac, E. A., and J. A. Lock, 1993: Calibration of the forward-scattering spectrometer probe: Modeling scattering from a multimode laser beam. *J. Atmos. Oceanic. Technol.,* **10,** 518–525.

Jones, A. S., and T. H. Vonder Haar, 1990: Passive microwave remote sensing of cloud liquid water over land regions. *J. Geophys. Res.,* **95,** 16 673–16 683.

King, M. D., 1987: Determination of the scaled optical thickness of clouds from reflected solar radiation measurements. *J. Atmos. Sci.,* **44,** 1734–1751.

Nakajima, T., and M. Tanaka, 1986: Matrix formulations for the transfer of solar radiation in a plane-parallel scattering atmosphere. *J. Quant. Spectrosc. Radiat. Transfer,* **35,** 13–21.

——, and ——, 1988: Algorithms for radiative intensity calculations in moderately thick atmospheres using a truncation approximation. *J. Quant. Spectrosc. Radiat. Transfer,* **40,** 51–69.

——, and M. D. King, 1990: Determination of the optical thickness and effective particle radius of clouds from reflected solar radiation measurements. Part I: Theory. *J. Atmos. Sci.,* **47,** 1878–1893.

——, ——, J. D. Spinhirne, and L. F. Radke, 1991: Determination of the optical thickness and effective particle radius of clouds from reflected solar radiation measurements. Part II: Marine stratocumulus observations. *J. Atmos. Sci.,* **48,** 728–750.

Prabhakara, C., A. T. C. Chang, and P. Gloersen, 1983: A statistical examination of *Nimbus-7* SMMR data and remote sensing of sea surface temperature, liquid water content in the atmosphere and surface wind speed. *J. Climate Appl. Meteor.,* **22,** 2023–2037.

Rawlins, F., and J. S. Foot, 1990: Remotely sensed measurements of stratocumulus properties during FIRE using the C130 aircraft multichannel radiometer. *J. Atmos. Sci.*, **47,** 2488–2503.

Rossow, W. B., 1989: Measuring cloud properties from space: A review. *J. Climate,* **2,** 201–213.

Slingo, A., S. Nicholls, and J. Schmetz, 1982: Aircraft observations of marine stratocumulus during JASIN. *Quart. J. Roy. Meteor. Soc.*, **108,** 833–856.

Spinhirne, J. D., R. Boers, and W. D. Hart, 1989: Cloud top liquid water from lidar observations of marine stratocumulus. *J. Appl. Meteor.*, **28,** 81–90.

Stephens, G. L., 1978: Radiation profiles in extended water clouds, II: Parameterization schemes. *J. Atmos. Sci.*, **35,** 2123–2132.

——, and S.-C. Tsay, 1990: On the cloud absorption anomaly. *Quart. J. Roy. Meteor. Soc.*, **116,** 671–704.

——, G. W. Paltridge, and C. M. R. Platt, 1978: Radiation profiles in extended water clouds, III: Observations. *J. Atmos. Sci.*, **35,** 2133–2141.

Takeda, T., and G. Liu, 1987: Estimation of atmospheric liquid-water amount by *Nimbus 7* SMMR data: A new method and its application to western North-Pacific region. *J. Meteor. Soc. Japan,* **65,** 931–947.

Wilheit, T. T., and A. T. C. Chang, 1980: An algorithm for retrieval of ocean surface and atmospheric parameters from the observations of the scanning multichannel microwave radiometer. *Radio Sci.*, **15,** 525–544.

Wu, M.-L., 1987: Determination of cloud ice water content and geometrical thickness using microwave and infrared radiometric measurements. *J. Climate Appl. Meteor.*, **26,** 878–884.